buildings

MDPI

Article

Progressive Failure Mechanism of Shield Tunnel Face in Complex Urban Geological Environment

Qingfei Huang [1] and Kaihang Han [2,3,*]

[1] CCCC Highway Consultants Co., Ltd., Beijing 100088, China; huangqingfei2022@126.com
[2] Shaanxi Provincial Key Laboratory of Highway Bridges and Tunnels, Chang'an University, Xi'an 710064, China
[3] Underground Polis Academy, Shenzhen University, Shenzhen 518060, China
* Correspondence: hankaihang@szu.edu.cn

Abstract: The construction of multiple tunnels across inland rivers has had a significant influence on the improvement of the transportation infrastructure. The technology for constructing tunnels is progressing towards the development of larger cross-sections, longer distances, and the ability to withstand high hydraulic pressure in complex hydrogeological conditions, including high-permeability strata. In order to ensure the face stability of shield tunnels under high hydraulic pressure that crosses a fault fracture zone, it is necessary to study the progressive failure mechanism of shield tunnel faces induced by high hydraulic pressure seepage. This paper employs finite element numerical simulation software to methodically examine the variation in the characteristics of the water seepage field, limiting support force, and face stability failure mode of shield tunnels passing through fault fracture zones with high hydraulic pressure under varying fault fracture width zones. The results show that the formation hydraulic gradient will progressively widen when the tunnel face is located within the undisturbed rock mass and is advanced towards the area of fault fracture. This will raise the likelihood of instability in the shield tunnel and progressively raise the limiting support force on the tunnel face. Moreover, as the tunnel face nears the region of fault fracture within the undisturbed rock mass, the damage range increases gradually. In addition, due to the increase in seepage force, the angle between the failure area and the horizontal plane becomes more and more gentle. On the contrary, as the tunnel's face moves closer to the undisturbed rock mass from the region of the fault fracture, the damage range gradually decreases, and the dip angle between the damage area and the horizontal plane becomes steeper and steeper due to the decreasing seepage force in the process. The study findings presented in this work are highly significant, both theoretically and practically, for the design and management of safety.

Keywords: shield tunnel; seepage field; spatial distribution; zone of fault fracture; high hydraulic pressure

Citation: Huang, Q.; Han, K. Progressive Failure Mechanism of Shield Tunnel Face in Complex Urban Geological Environment. *Buildings* **2024**, *14*, 1356. https://doi.org/10.3390/buildings14051356

Academic Editor: Yong Tan

Received: 15 November 2023
Revised: 19 December 2023
Accepted: 21 December 2023
Published: 10 May 2024

1. Introduction

The construction of a tunnel between two cities offers a direct connection, circumventing the need for detours sometimes encountered in conventional land transportation. Consequently, this infrastructure development reduces the distance between the cities and enhances overall traffic efficiency [1–4]. Transport vehicles can be directly carried to their destination through underwater tunnels or submarine pipelines, thereby circumventing issues such as congestion and traffic accidents commonly encountered in land traffic. This mode of transportation enhances both efficiency and safety in traffic operations. Simultaneously, the implementation of several tunnels can effectively augment traffic capacity in order to accommodate the escalating traffic demand between urban areas. The tunnel does not occupy spatial dimensions, impede navigation, or impact the natural environment, and serves as a secure and reliable all-weather conduit [5–7]. The construction of the tunnel has

the potential to facilitate regional economic development, enhance intercity connectivity and collaboration, and enhance the overall economic competitiveness of the region. In summary, the establishment of the tunnel holds considerable importance in facilitating economic progress, enhancing the quality of life for individuals, and optimizing transportation efficacy [8–12]. Figure 1 displays a typical engineering project for an underwater tunnel traversing several zones of fault fractures with high hydraulic pressure.

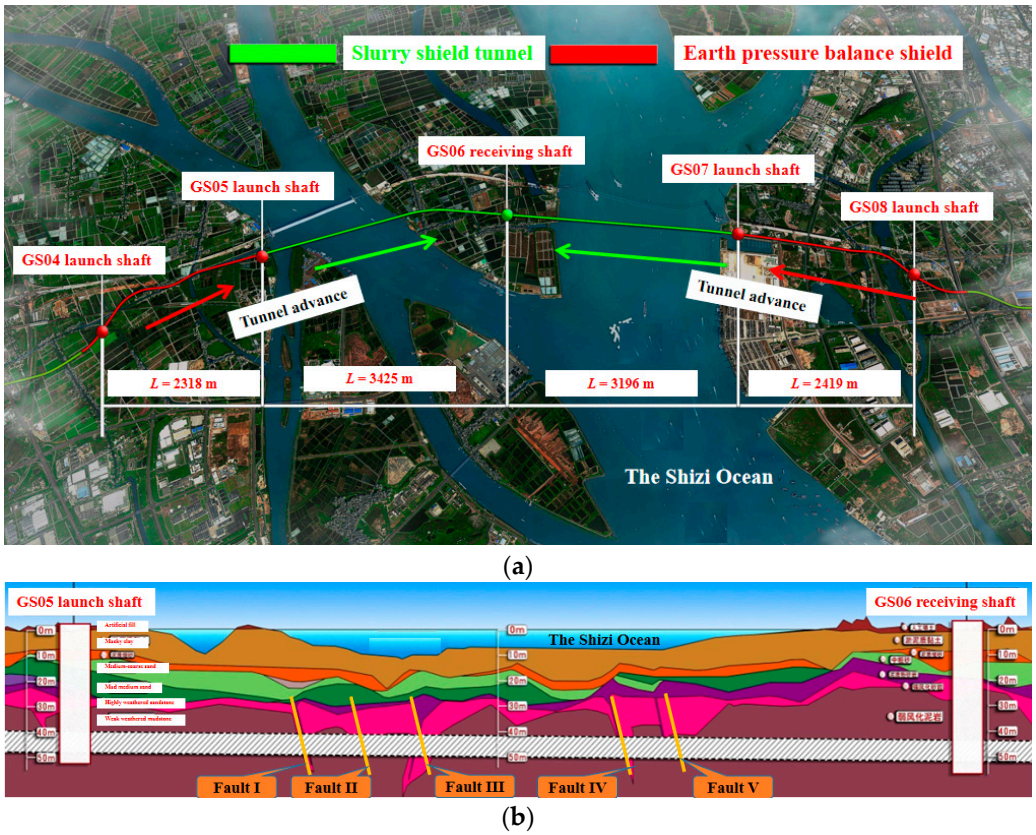

Figure 1. A tunnel engineering project with several zone of fault fractures with high hydraulic pressure. (**a**) Plan view of project site; (**b**) Geological profile.

Typically, researchers employ numerical simulations, model experiments or theoretical analysis to study the gradual instability process of tunnel-surrounding rock. (1) Theoretical Analysis. The notion of unsaturated transient flow was developed by Hou and Yang (2022) [13] in their investigation of tunnel face stability. They integrated this concept into a three-dimensional (3D) framework and employed a closed-form approach to characterize the variability of saturation, suction stress, and apparent cohesiveness in soils that are partially saturated. The equation for work rate balance, which incorporates the unsaturated component, was derived utilizing a three-dimensional horn-shaped failure mechanism. Their results show that the required face pressure decreases when unsaturated transient flows are used. In particular, there was a 16.22% decrease in fine sands, a 24.98% decrease in silts, and an 85.62% decrease in clays. The impact of weak interlayer and rock layer inclination on tunnel face stability was examined in the study by Man et al. (2022) [14]. In order to achieve virtual supporting force, they employed the upper limit theorem and the genetic algorithm. These methods showed that an increase in instability is caused by a weak interlayer container, lower-layer features, and inadequate interlayer location and thickness. They also highlighted the crucial angle related to the rock strata' slope. In order to facilitate safety evaluations and engineering design, Park (2023) [15] carried out a thorough analysis to investigate the analytical solution relevant to the characterization of tunnel roof collapse profiles and estimated stability measures. Considerations for pore

pressure, seismic excitation, shallow depth, and axis-symmetric analysis were added to the methodology. The development of original and expanded mathematical formulas yielded the optimal limits for the stability number, factor of safety based on shear strength, and support pressure. The numerical results demonstrated excellent agreement with semi-analytical and numerical approaches, presenting improved solutions designed for shallow tunnels. Tu et al. (2023) [16] refined a 3D rotating rigid body collapse mechanism for designated layered soils using a discretization technique, improving the study of tunnel face stability during excavation in inclined soil. The present study's methodology sheds light on the existence of asymmetric failure mechanisms and the fluctuations in active failure pressure. The amount of surface sinking is also influenced by the terrain's inclination. Li et al. (2023) [17] looked at how stable faces were during shield tunneling in sloping strata. Numerical simulation methods were used with theoretical analysis to conduct this inquiry. The goal of this research is to present a thorough three-dimensional (3D) kinematic failure process, with an emphasis on the junction of the tunnel face and an inclined soil contact. This study looks into how a geological face's stability is affected by the location and dip of inclined layers. (2) Model Experiments. Using a 3D printing model, Li et al. (2022) [18] investigated the deformation behavior of the invert of operating railway tunnels. Six distinct experimental groups were created in order to investigate the impact of environmental factors in addition to design elements. When comparing optimal drainage systems (ODS) to traditional drainage systems (TDS), the results showed significant differences in water outflow, effective water permeability (EWP), and invert stability. Excessive external water pressure (EWP) below the invert is difficult for the TDS method to control, but the ODS approach shows that it can control EWP at the tunnel base, which means that the invert can remain stable even when blind tubes are blocked. Di et al. (2023) [19] looked at how relative density affects shield tunnel stability in sandstone cobble strata. Samples with varied degrees of compaction, such as loose, moderately dense, and dense samples, were used in geomechanical model tests. The study's conclusions show that, in the context of tunnel instability, there is a significant relationship between relative density and horizontal ground pressure. More specifically, it was found that density increases improve the lateral pressure coefficient, which in turn increases tunnel face stability. This paper provides a thorough examination of shield tunnel engineering in strata with sand-cobbles, emphasizing the disparities seen in existing approaches. An adaptive image update strategy was proposed by Jia et al. (2023) [20] with the goal of improving the threshold update approach used in PIV processing and producing better post-processed images. The failure mechanism of tunnel faces in clay strata is examined in this work, with particular attention paid to the impacts of different longitudinal inclination degrees and the buried depth to diameter ratio. The results show the existence of an ellipsoid failure form, which is linked to a higher chance of collapse in situations when the inclination angle is upward and the burial depth is shallow. This means that prolonged upward-sloped excavation inside clay strata should be avoided. (3) Numerical Simulations. The combination of the unique element approach and terrestrial laser scanning (TLS) was utilized by Wang et al. (2023) [21] to evaluate the properties of rock masses and examine their stability in tunnel environments. Without requiring direct contact, TLS technology may obtain exact geometry data of the surrounding rock mass. Furthermore, a new algorithm has been created to automatically detect breaks in the recorded data. This technology is more accurate and efficient than manual mapping procedures because it allows the visual identification of discontinuities and characteristics of spatial distribution. After a structural breakdown, the approach was used to locate unstable rock masses in the spillway and sand flushing tunnel of the Hongshiyan hydropower facility. This approach is a useful tool for carrying out geological surveys and reducing the hazards related to unstable rock blocks in tunnel settings. Nguyen-Minh et al. (2023) [22] evaluated the stability of a rectangular tunnel in undrained clay during the lining procedure. A formulation of an upper bound limit analysis along with isogeometric analysis (IGA) are used in the stability investigation. The geometric representation is achieved by using B-spline basis functions,

and the upper bound limit analysis is formulated as a second-order cone program (SOCP) using a numerical optimization technique. Comparing the results with those from previous research allows for an evaluation of the procedure's accuracy and reliability. The suggested approach provides a comprehensive and reliable solution for evaluating the stability of rectangular tunnels, providing accurate results at the same time as reducing computing costs. Keawsawasvong and Ukritcho (2022) [23] performed a study with the objective of investigating the effects of strength nonhomogeneity and undrained strength anisotropy on the stability of unlined circular tunnels in clay formations. This study revealed a non-linear link between the stability load factor and the ratio of cover depth through the application of lower-bound analysis. It also showed that the normalized overburden pressure and the strength gradient are linearly related to the stability load factor. An innovative stability equation for unlined circular tunnels in anisotropic and non-homogeneous clay is presented in this study. Four more terms are included in the equation: soil unit weight, undrained strength anisotropy, linearly increasing strength gradient, and constant undrained strength. Tu et al. (2023) [24] used a two-phase single-point material point method (MPM) to study a saturated stratum's hydro-mechanical properties and failure development. The approach has been shown effective, and studies into the critical support pressure, failure mechanism, and post-failure mechanisms have been conducted using simulations. The results show that the material point method (MPM) can be used to predict tunnel face failure with high accuracy, providing important information for the creation of practical tunnel designs. A well-developed predictive model was proposed by Li et al. (2023) [25] to estimate the limit support pressure of underwater tunnel sides. Their main goal in the research was to reduce the likelihood of any injury. The model uses numerical simulations and mechanical analysis to determine the main factors affecting the pressure. It has been established that the support vector machine (SVM) model is effective for predicting limit support pressure, which implies that it may find use in other engineering contexts.

Nonetheless, there are a number of major problems with this study. In particular, pore water pressure dissipation causes a notable increase in hydraulic gradient, seepage velocity, and seepage dynamic water pressure when the tunnel passes through the fault fracture zone. As a result, groundwater is more likely to flow in the direction of the tunnel's tunnel face, increasing the possibility of instability there. However, there is a paucity of thorough research about the methodical examination of the seepage field distribution near the tunnel face of a stratum tunnel across a fault fracture zone. In this paper, the distribution characteristics of seepage field, limiting support force, and failure mode of face stability of a shield tunnel passing through the high hydraulic pressure zone of a fault fracture under different width zones of the fault fracture are systematically studied using finite element numerical simulation software.

2. Finite Element Numerical Simulation

The program utilized in this work, PLAXIS 3D, demonstrates exceptional proficiency in precisely replicating tunnel excavation, fluid–structure interaction, and deformation of geological formations within the realm of geotechnical engineering. As seen in Figure 2, the numerical model has the following dimensions: length (along y axis) = 100 m; width (along x axis) = 50 m; and depth (along z axis) = 50 m. The tunnel's diameter is 10 m. Gravity accelerates at a rate of 9.8 m/s squared along the -z axis. The top surface of the model is subjected to a stress boundary condition, while a uniform load of 1 MPa is supplied to replicate the pressure exerted on the bottom surface of the sea floor by a 100 m thick layer of seawater. Due to the adoption of the symmetric approach in the numerical simulation model, only half of the tunnel model was constructed. As a result, the right side of the model was subjected to a rolling boundary condition, which prevented displacement in the x direction. The remaining three sides of the model similarly had rolling boundary conditions, and the methods for enforcing constraints were similar. The lower part of the model was subject to a fixed boundary condition.

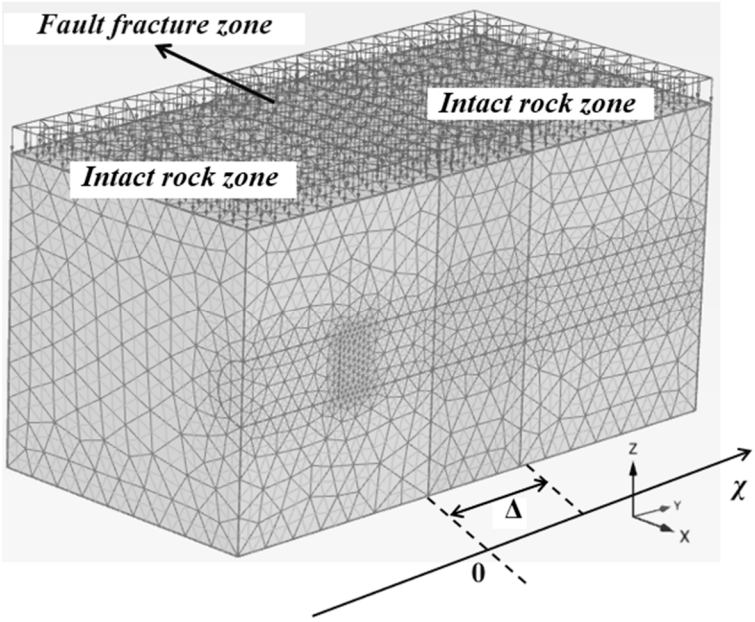

Figure 2. Finite element numerical simulation model.

This paper focuses on the failure mode and limiting support force of a tunnel face. Therefore, the specific process of tunnel excavation and support was ignored in the simulation, and the units within the tunnel were deleted once, and the tunnel support structure was set up. The tunnel face is subjected to trapezoidal distributed loads, which will be correspondingly lowered to simulate the instability of the tunnel face. Despite the use of a simplified simulation method, the instability process of the tunnel face closely resembles that of real-world engineering scenarios. The stress–displacement relationship curve is created by extracting the horizontal displacement and horizontal stress data from the center point of the tunnel face. To replicate the most difficult construction circumstances, the tunnel face chamber's water head was adjusted to 0 m. The rock's strength was determined by the Mohr Coulomb strength criterion. The fluid–structure coupling analysis approach was utilized. Table 1 displays the mechanical and physical characteristics of the strata employed in the numerical simulation. In order to study the influence of the width of the zone of fault fracture on the limiting support force, the width of the zone of fault fracture was set as 5 m, 10 m, 15 m and 20 m, respectively. The selection of the tunnel face location χ is the most representative of the spatial correlations between the fault fracture zone and the tunnel face (χ= −2 D, −1 D, −0.5 D, −0.25 D, 0 D, 1 D, 1.5 D, and 2 D).

Table 1. Soil parameters.

Parameters	Undisturbed Rock Mass	Zone of Fault Fracture
γ_{unsat} [kN/m^3]	19.50	18.50
γ_{sat} [kN/m^3]	20.50	19.50
E [kN/m^2]	50×10^3	10×10^3
ν (nu)	0.2	0.3
G [kN/m^2]	20.83×10^3	3846
C [kN/m^2]	300	50
φ (phi) [°]	25	10
K_0	0.5774	0.8264
K [m/day]	0.00173	0.173

3. Numerical Simulation Results

3.1. Analysis of Characteristics of Formation Seepage Field

The distribution patterns of the formation water head in the limit state are depicted in Figure 3. The distribution patterns of pore water pressure under the limit state are shown in Figure 4 when the tunnel face is at the location χ = 1.0 D.

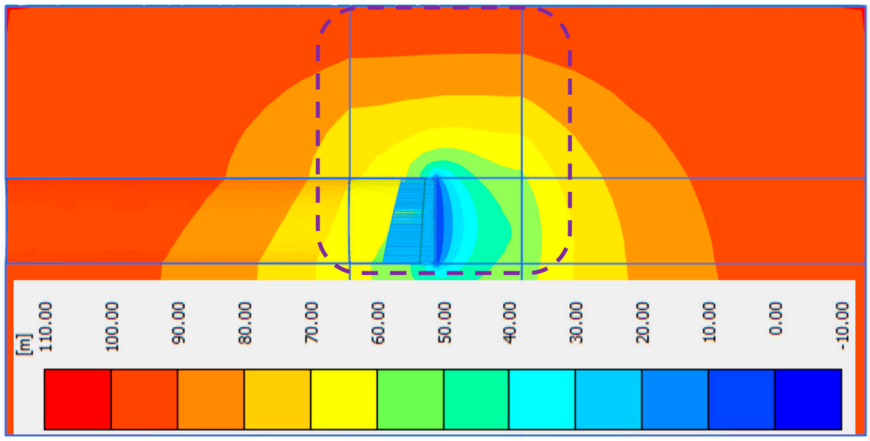

Figure 3. Nephogram of water head distribution at the position of tunnel face under limit state [χ = 1.0 D].

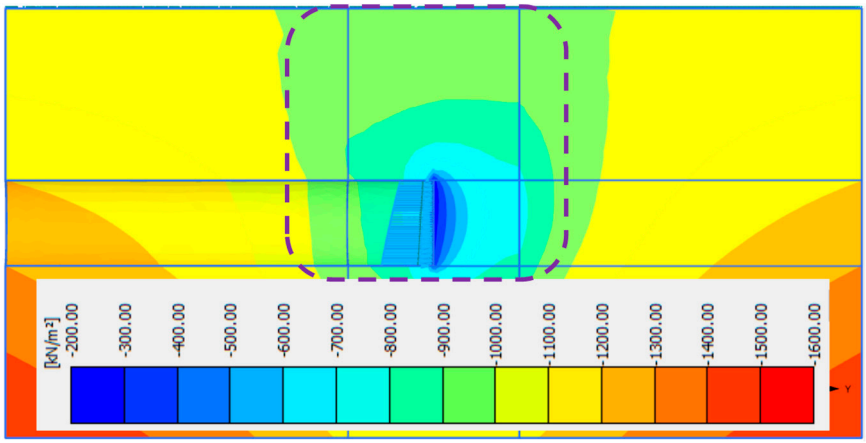

Figure 4. Distribution nephogram of pore water pressure at the position of tunnel face under limit state [χ = 1.0 D].

The findings demonstrate that when the tunnel face moves closer to the zone of fault fracture from the undisturbed rock mass, the equivalent nephogram of formation water head and pore water pressure becomes denser and denser, indicating an increasing hydraulic gradient. Conversely, as the tunnel face moves closer to the undisturbed rock mass from the fault fracture zone, the hydraulic gradient becomes lower and smaller, and the equivalent nephogram of the formation water head and pore water pressure becomes sparser. These findings are in line with the independent seepage analysis rule and the findings reported in the body of current research.

The nephogram of the hydraulic gradient distribution in the limit condition is displayed in Figure 5. The findings indicate that the hydraulic gradient of the stratum close to the tunnel face increases as the tunnel moves closer to the zone of fault fracture. The hydraulic gradient of the stratum close to the tunnel face decreases as the tunnel moves through the fault fracture zone.

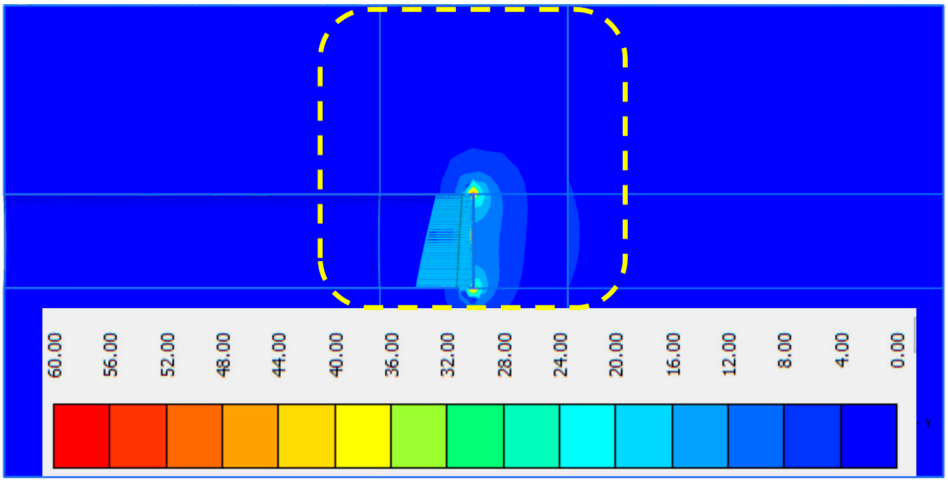

Figure 5. Distribution nephogram of hydraulic gradient at the position of tunnel face under limit state [χ = 1.0 D].

The hydraulic gradient variation rules on horizontal and vertical monitoring lines at various tunnel face sites are presented in Figures 6 and 7, respectively, based on the outcomes of the numerical simulation. The formation hydraulic gradient grows larger and larger when the tunnel face is situated in the undisturbed rock mass and is driven toward the zone of fault fracture, as shown in Figures 6 and 7. This will progressively raise the shield tunnel face's limiting support force and raise the likelihood of the tunnel becoming unstable. Conversely, the hydraulic gradient gradually decreases as the tunnel is driven toward the undisturbed rock mass and the tunnel face is situated in the fault fracture zone. This reduces the limiting support force of the shield tunnel face and promotes the stability of the tunnel face.

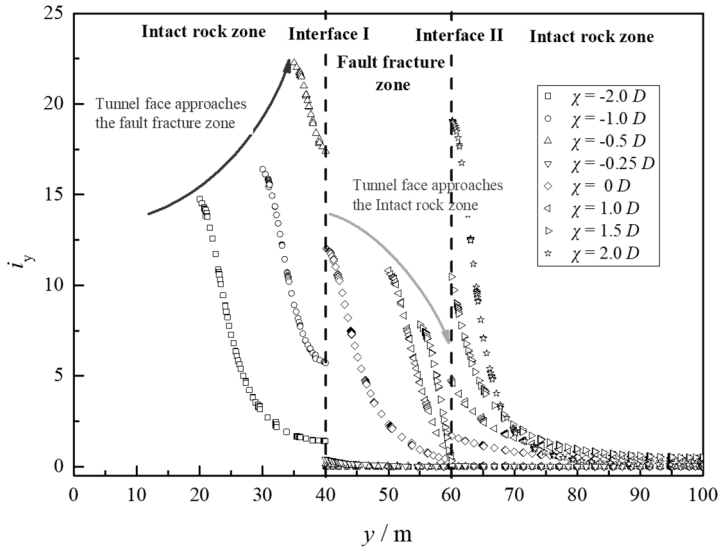

Figure 6. Hydraulic gradients on measurement lines at different distances from launching planes.

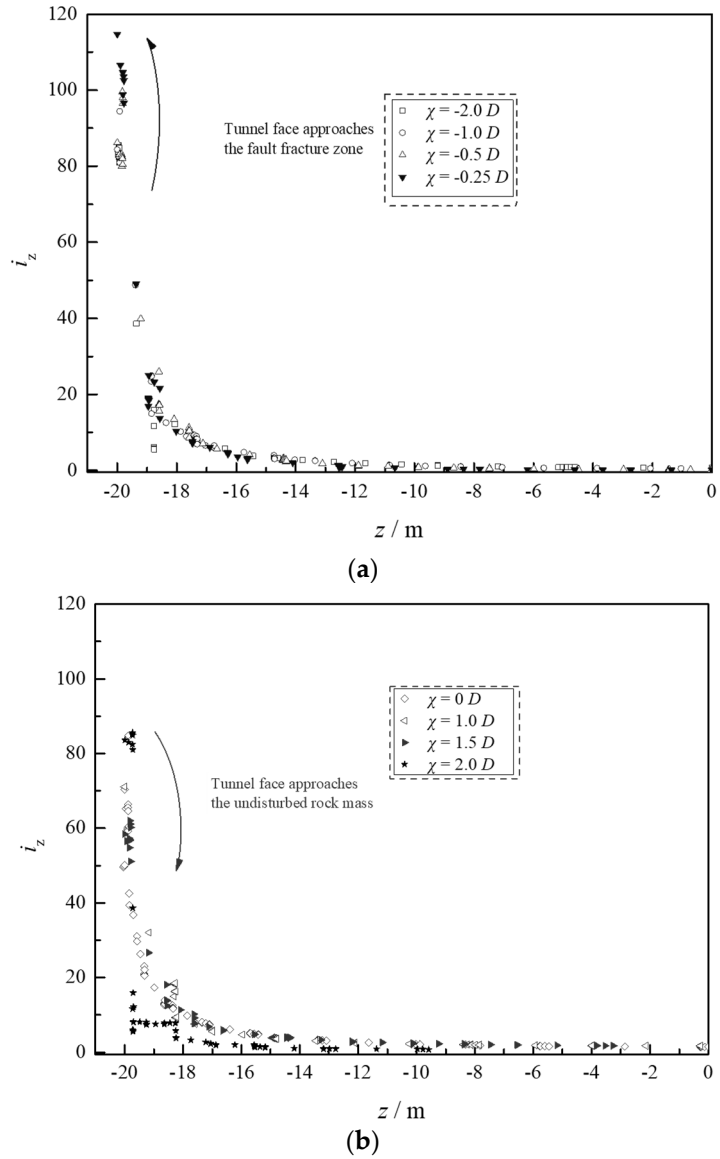

Figure 7. Hydraulic gradients on vertical measuring lines at different distances: (**a**) when the tunnel face is advanced towards the fault fracture zone; (**b**) when the tunnel face is advanced towards the area of undisturbed rock mass.

3.2. Analysis of the Change Law of Limit Supporting Force

Figure 8 displays the relationship curve between horizontal displacement and horizontal stress at the center of the tunnel face based on the outcomes of the numerical simulation. The horizontal displacement at the center of the tunnel face is zero when the trapezoidal distribution pressure equals the starting earth pressure. The horizontal displacement of the tunnel face's central point node grows with a steady reduction in trapezoidal distribution pressure. Even a slight reduction in support pressure will cause the horizontal displacement of the tunnel face's central point node to increase sharply until the calculation fails to converge, indicating that the shield tunnel face has become unstable. This process occurs when the support pressure of the tunnel face falls to a certain value. Thus, the final supporting force is defined as the supporting pressure of the tunnel face.

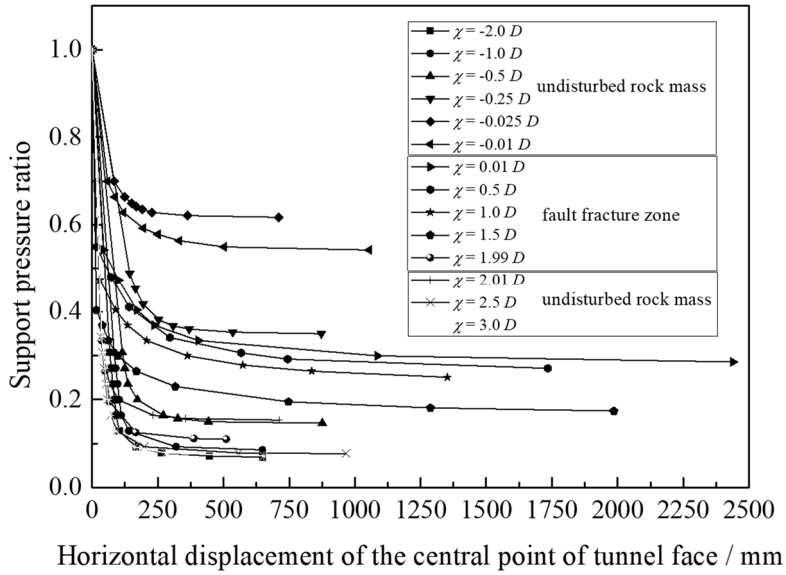

Figure 8. Relation between horizontal displacement and support pressure ratio (L = 2.0 D).

Figure 9 illustrates the link between the limiting support pressure ratio and varied distance χ based on the outcomes of numerical simulation. The limiting support force is unaffected by the zone of fault fracture when the tunnel face is located far from it. Additionally, the limiting support force is negligible because of the undisturbed rock mass's considerable strength. The limiting support force grows quickly as the distance from the initial contact gradually becomes smaller; at its maximum, it is around six times more than the limiting support force of the undisturbed rock mass. The shield tunnel passes through the initial interface, and then there is a significant decline in the limiting support force. The final sustaining pressure of the fault fracture zone is higher than that of the undisturbed rock mass due to the comparatively low inner layer strength. In order to prevent water gushing and mud outburst mishaps, the supporting pressure of the tunnel face should be tightly managed at this point. The impact of the fault fracture zone width on the variation in the limiting support pressure is also seen in Figure 9. The findings demonstrate that, for fault fracture zones of varying widths, the fluctuation trend in the limiting support pressure is identical. The limiting support force significantly decreases when the tunnel face passes through the interface and the width of the fault fracture zone is minimal (Δ = 0.5 D).

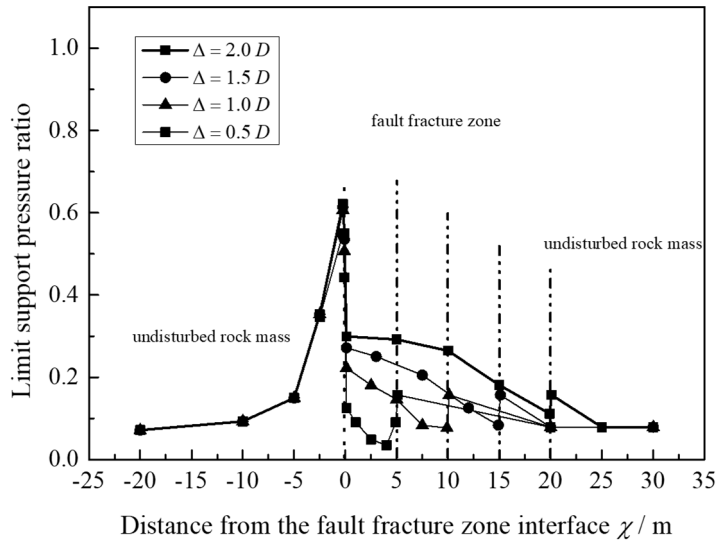

Figure 9. Influence of the width of zone of fault fracture on the variation of limiting support force.

3.3. Analysis of the Change Law of Failure Mode

The formation displacement nephogram under the limit state is shown in Figure 10 at the location along the tunnel face [χ = 1.0 D]. When the tunnel face passes through the zone of fault fracture at various points, the findings show the development law of the failure mode of the surrounding rock in front of the tunnel excavation under the limit state. Since the undisturbed rock mass's mechanical characteristics are superior to those of the fault fracture zone, its failure range is often narrower than that of the strata in the zone of fault fracture. The failure range rapidly rises as the tunnel face moves from the undisturbed rock bulk toward the zone of fault fracture. Furthermore, the angle between the failure region and the horizontal plane becomes increasingly mild as permeability increases. Conversely, the failure range rapidly decreases as the tunnel face approaches the undisturbed rock mass from the fault fracture zone. The process's diminishing permeability causes the dip angle between the horizontal plane and the failure region to steepen more and more.

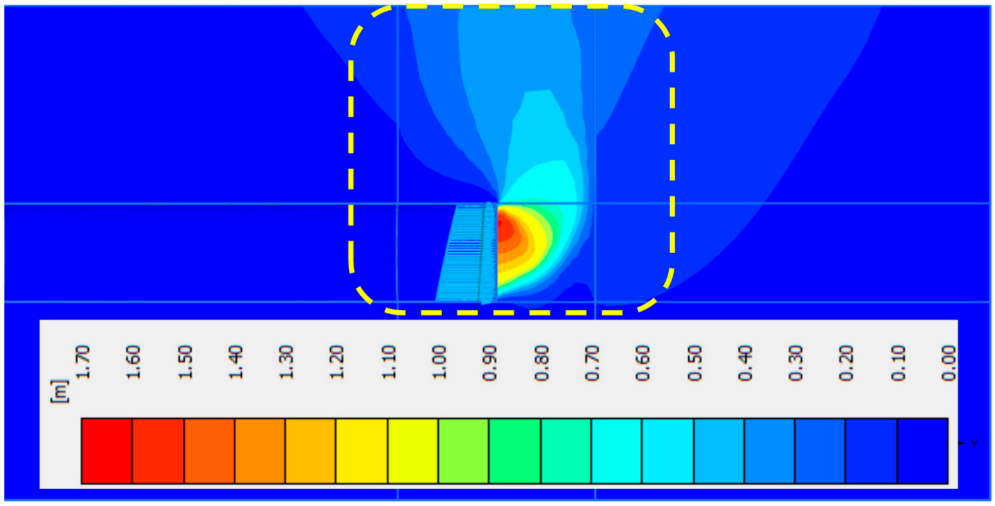

Figure 10. Nephogram of stratum displacement distribution at different positions of tunnel face under limit state [χ = 1.0 D].

Figure 11 illustrates how the area with surface displacement of more than 0.3 m was extracted and the displacement contour line was created based on the outcomes of the numerical simulation and model test. The failure zone boundary was found to be between 0.3 m (3% D) and 0.53 m (5.3% D). When the tunnel face passes through the zone of fault fracture at various points, the findings show the development law of the failure mode of the surrounding rock in front of the tunnel excavation under the limit state. Since the undisturbed rock mass's mechanical characteristics are superior to those of the fault fracture zone, its failure range is often narrower than that of the strata in the zone of fault fracture. The failure range rapidly rises as the tunnel face moves from the undisturbed rock bulk toward the zone of fault fracture. Furthermore, the angle between the failure region and the horizontal plane becomes increasingly mild as permeability increases. Conversely, the failure range rapidly decreases as the tunnel face approaches the undisturbed rock mass from the fault fracture zone. The process's diminishing permeability causes the dip angle between the horizontal plane and the failure region to steepen more and more.

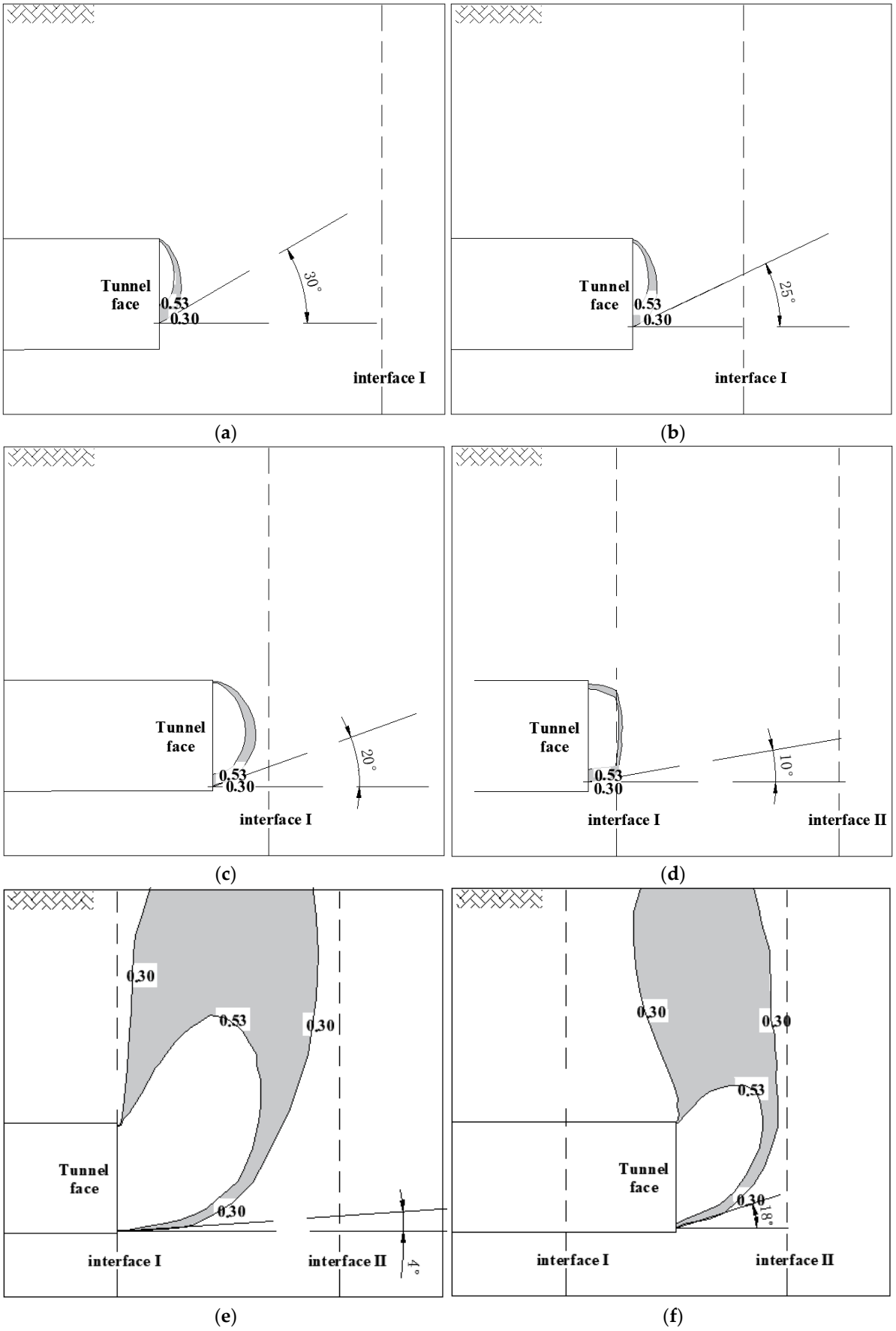

Figure 11. *Cont.*

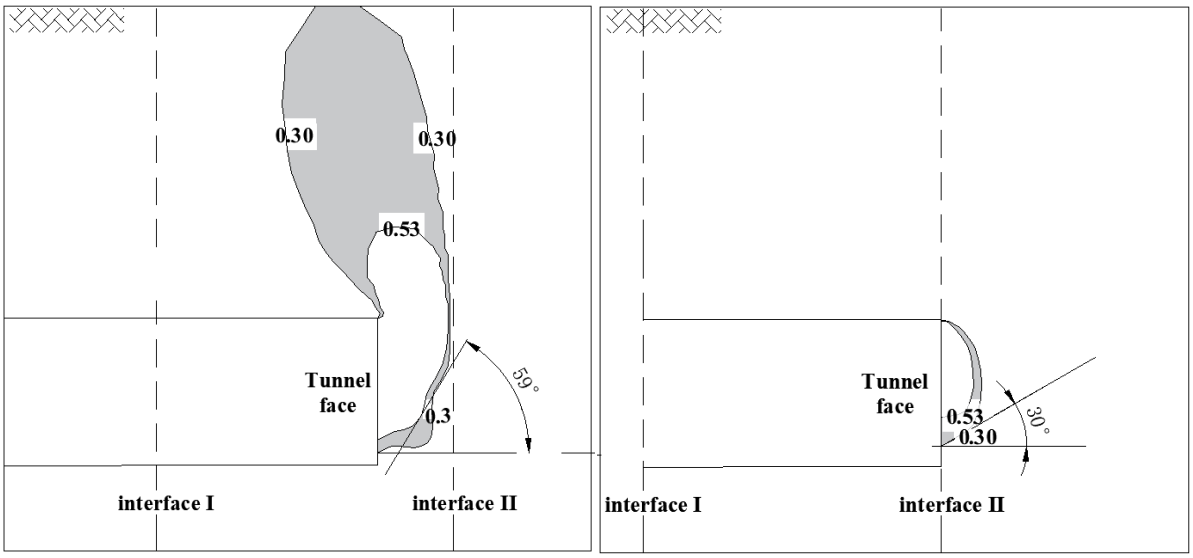

Figure 11. Failure zone boundary at different positions of tunnel face in limit state. (**a**) $\chi = -2.0$ D; (**b**) $\chi = -1.0$ D; (**c**) $\chi = -0.5$ D; (**d**) $\chi = -0.25$ D; (**e**)$\chi = 0$ D; (**f**) $\chi = 1.0$ D; (**g**) $\chi = 1.5$ D; (**h**) $\chi = 2.0$ D.

Figure 12 displays the critical inclination angle βcr at various points of the tunnel face in the limit condition. The critical inclination angle of the failure zone is constant and exhibits a horizontal trend when the tunnel face is distant from the fault fracture zone. The lower portion of the failure area will also become flat as the tunnel face moves closer to the zone of fault fracture as a result of the progressive rise in horizontal permeability, and at this point, the critical inclination angle of the failure region displays a downward trend. In contrast, the lower portion of the failure area will likewise become steep due to the gradual decrease in horizontal permeability when the tunnel face is situated in the zone of fault fracture and approaches the undisturbed rock mass area. At this point, the critical inclination angle of the failure area shows an upward trend. Ultimately, the critical inclination angle remains constant and exhibits a horizontal trend when the tunnel traverses the fault fracture zone, where the failure region is located in the undisturbed rock mass.

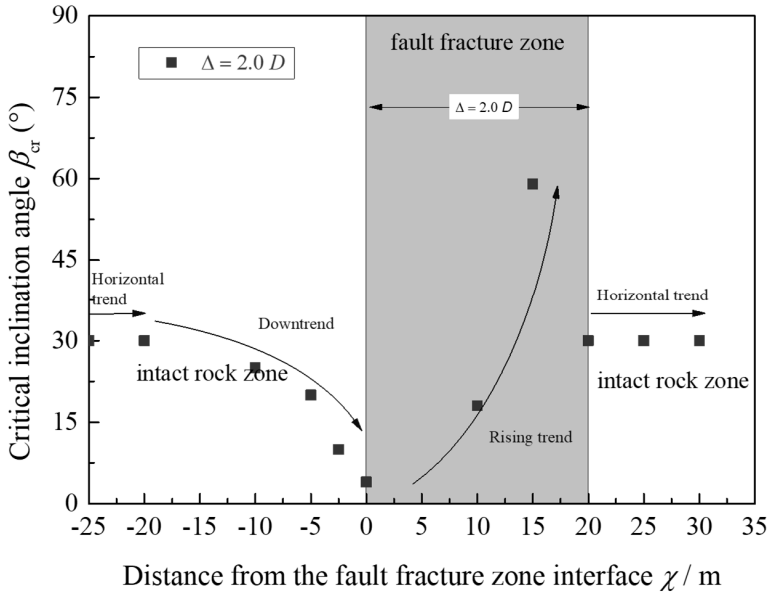

Figure 12. Critical inclination angle βcr with different locations of the tunnel face in the limit state.

4. Conclusions

The distribution characteristics of the seepage field, limiting support force, and failure mode of tunnel face stability of a shield tunnel passing through the high hydraulic zone of a fault fracture with different widths were systematically studied in this paper based on numerical simulation, model tests, and functional mutation theory analysis. The following are the primary conclusions:

(1) The formation hydraulic gradient gradually increases as the tunnel face moves toward the zone of fault fracture while it remains in the undisturbed rock mass. This will raise the likelihood of the shield tunnel becoming unstable and progressively increase the ultimate support force of the tunnel face. Conversely, the hydraulic gradient gradually decreases as the tunnel is driven toward the undisturbed rock mass and the tunnel face is situated in the fault fracture zone. This reduces the ultimate supporting force of the shield tunnel face and promotes the stability of the tunnel face.

(2) The limiting support force is not impacted by the zone of fault fracture when the tunnel face is distant from the fault fracture. Additionally, the limiting support force is negligible because of the undisturbed rock mass's considerable strength. The limiting support force grows quickly as the distance from the initial contact progressively becomes smaller; at its maximum, it is around six times more than the limiting support force of the undisturbed rock mass. The shield tunnel passes through the initial interface, and then there is a significant decline in the limiting support force. The final sustaining pressure of the fault fracture zone is greater than that of the undisturbed rock mass due to the comparatively low inner layer strength. In order to prevent water gushing and mud outburst mishaps, the supporting pressure of the tunnel face should be tightly managed at this point.

(3) The investigation into how the width of the fault fracture zone affects the variation in the limiting support pressure reveals that the limiting support pressure fluctuation trend is consistent across fault fracture zones of various widths. The limiting support force significantly decreases when the tunnel face passes through the interface and the width of the fault fracture zone is minimal (Δ = 0.5 D).

(4) After extracting the area with a surface displacement of more than 0.3 m, the displacement contour line was created. A range of 0.3 m (3% D) to 0.53 m (5.3% D) was identified as the failure zone's perimeter. The findings indicate that since the mechanical properties of the undisturbed rock mass are superior to those of the zone of fault fracture, the failure range of the former is often less than that of the latter. The failure range rapidly rises as the tunnel face moves from the undisturbed rock bulk toward the zone of fault fracture. Furthermore, the angle between the failure region and the horizontal plane becomes increasingly mild as permeability increases. Conversely, the failure range rapidly decreases as the tunnel face approaches the undisturbed rock mass from the fault fracture zone. The process's diminishing permeability causes the dip angle between the horizontal plane and the failure region to steepen more and more.

This paper focused on the progressive failure process of a shield tunnel face in a complicated urban geological environment. Nevertheless, practical engineering must take into account aspects such as cutter head rotation and the unstable seepage state of the formation, which will be the subjects of future research.

Author Contributions: Conceptualization, K.H.; methodology, K.H.; software, Q.H.; validation, Q.H. and K.H.; formal analysis, Q.H. and K.H; investigation, Q.H. and K.H.; resources, Q.H. and K.H.; data curation, Q.H. and K.H.; writing—original draft preparation, Q.H. and K.H.; writing-review and editing, K.H.; visualization, K.H.; supervision, K.H.; project administration, K.H.; funding acquisition, K.H. All authors have read and agreed to the published version of the manuscript.

Funding: This research was funded by the National Natural Science Foundation of China (Grant No. 51908371) and the Fundamental Research Funds for the Central Universities (Grant No. 300102211516).

Data Availability Statement: The data that support the findings of this study are available within the manuscript.

Conflicts of Interest: The authors declare no conflicts of interest.

References

1. Han, K.; Wang, L.; Su, D.; Hong, C.; Chen, X.; Lin, X.T. An analytical model for face stability of tunnels traversing the fault fracture zone with high hydraulic pressure. *Comput. Geotech.* **2021**, *140*, 104467. [CrossRef]
2. Habumuremyi, P.; Xiang, Y. A 3-D analytical continuous upper bound limit analysis for face stability of shallow shield tunneling in undrained clays. *Comput. Geotech.* **2023**, *164*, 105779. [CrossRef]
3. Huang, M.; Lu, Y.; Zhen, J.; Lan, X.; Xu, C.; Yu, W. Analysis of face stability at the launch stage of shield or TBM tunnelling using a concrete box in complex urban environments. *Tunn. Undergr. Space Technol.* **2023**, *135*, 105067. [CrossRef]
4. Di, Q.; Li, P.; Zhang, M.; Zhang, W.; Wang, X. Analysis of face stability for tunnels under seepage flow in the saturated ground. *Ocean Eng.* **2022**, *266*, 112674. [CrossRef]
5. Man, J.; Zhou, M.; Zhang, D.; Huang, H.; Chen, J. Face stability analysis of circular tunnels in layered rock masses using the upper bound theorem. *J. Rock Mech. Geotech. Eng.* **2022**, *14*, 1836–1848. [CrossRef]
6. Ding, X.; Li, K.; Xie, Y.; Liu, S. Face stability analysis of large shield-driven tunnel in rock-soil interface composite formations. *Undergr. Space* **2022**, *7*, 1021–1035. [CrossRef]
7. Hao, X.; Yuan, L.; Sun, Z.; Zhao, Y.; Ren, B.; Zhao, D.; Xue, J.; Zhang, X.; Yu, G.; Zhang, Q. An integrated study of physical and numerical modelling on the stability of underground tunnel influenced by unloading rate. *Tunn. Undergr. Space Technol.* **2022**, *129*, 104602. [CrossRef]
8. Li, X.; Zhu, Z.; Wang, M.; Shu, Y.; Deng, S.; Xiao, D. Influence of blasting load directions on tunnel stability in fractured rock mass. *J. Rock Mech. Geotech. Eng.* **2022**, *14*, 346–365. [CrossRef]
9. Han, K.; Zhang, D.; Chen, X.; Su, D.; Ju, J.-W.W.; Lin, X.-T.; Cui, H. A resilience assessment framework for existing underground structures under adjacent construction disturbance. *Tunn. Undergr. Space Technol. Inc. Trenchless Technol. Res.* **2023**, *141*, 105339. [CrossRef]
10. Huang, F.; Shi, X.; Wu, C.; Dong, G.; Liu, X.; Zheng, A. Stability analysis of tunnel under coal seam goaf: Numerical and physical modeling. *Undergr. Space* **2023**, *11*, 246–261. [CrossRef]
11. Xu, X.; He, M.; Zhu, C.; Lin, Y.; Cao, C. A new calculation model of blasting damage degree-Based on fractal and tie rod damage theory. *Eng. Fract. Mech.* **2019**, *220*, 106619. [CrossRef]
12. Li, G.; Zhu, C.; Tang, S.; Dun, K.; Wu, C. Energy balance support method in soft rock tunnel with energy absorbing anchor cable. *Tunn. Undergr. Space Technol.* **2023**, *141*, 105380. [CrossRef]
13. Hou, C.T.; Yang, X.L. 3D stability analysis of tunnel face with influence of unsaturated transient flow. *Tunn. Undergr. Space Technol.* **2022**, *123*, 104414. [CrossRef]
14. Man, J.; Huang, H.; Ai, Z.; Chen, J. Analytical model for tunnel face stability in longitudinally inclined layered rock masses with weak interlayer. *Comput. Geotech.* **2022**, *143*, 104608. [CrossRef]
15. Park, D. Complementation of analytical solutions for the quantitative roof stability analysis of rock cavities and tunnels. *Int. J. Rock Mech. Min. Sci.* **2023**, *170*, 105556. [CrossRef]
16. Tu, S.; Li, W.; Zhang, C.; Chen, W. Effect of inclined layered soils on face stability in shield tunneling based on limit analysis. *Tunn. Undergr. Space Technol.* **2023**, *131*, 104773. [CrossRef]
17. Li, W.; Zhang, C.; Tu, S.; Chen, W.; Ma, M. Face stability analysis of a shield tunnel excavated along inclined strata. *Undergr. Space* **2023**, *13*, 183–204. [CrossRef]
18. Li, L.; Yang, J.; Fu, J.; Wang, S.; Zhang, C.; Xiang, M. Experimental investigation on the invert stability of operating railway tunnels with different drainage systems using 3D printing technology. *J. Rock Mech. Geotech. Eng.* **2022**, *14*, 1470–1485. [CrossRef]
19. Di, Q.; Li, P.; Zhang, M.; Cui, X. Experimental study of face stability for shield tunnels in sandy cobble strata of different densities. *Tunn. Undergr. Space Technol.* **2023**, *135*, 105029. [CrossRef]
20. Jia, Z.; Bai, Y.; Liu, C.; Zhang, D.; Ji, Y.; Zhao, H. Visualization investigation on stability of shield tunnel face with transparent soil, considering different longitudinal inclination angles. *Tunn. Undergr. Space Technol.* **2023**, *137*, 105154. [CrossRef]
21. Wang, M.; Zhou, J.; Chen, J.; Jiang, N.; Zhang, P.; Li, H. Automatic identification of rock discontinuity and stability analysis of tunnel rock blocks using terrestrial laser scanning. *J. Rock Mech. Geotech. Eng.* **2023**, *15*, 1810–1825. [CrossRef]
22. Nguyen-Minh, T.; Bui-Ngoc, T.; Shiau, J.; Nguyen, T.; Nguyen-Thoi, T. Coupling isogeometric analysis with deep learning for stability evaluation of rectangular tunnels. *Tunn. Undergr. Space Technol.* **2023**, *140*, 105330. [CrossRef]
23. Keawsawasvong, S.; Ukritchon, B. Design equation for stability of a circular tunnel in anisotropic and heterogeneous clay. *Undergr. Space* **2022**, *7*, 76–93. [CrossRef]

24. Tu, S.; Li, W.; Zhang, C.; Wang, L.; Wang, S.; Zhao, Y.; Wu, J. Face stability analysis of tunnels in saturated soil considering soil-fluid coupling effect via material point method. *Comput. Geotech.* **2023**, *161*, 105592. [CrossRef]
25. Li, X.; Xue, Y.; Li, Z.; Kong, F.; Li, G.; Zhou, B. Numerical investigation and prediction of the excavation face stability for river-crossing shield tunneling: An intelligent prediction model for limit support pressure. *Comput. Geotech.* **2023**, *160*, 105493. [CrossRef]